






Cite this: *Chem. Sci.*, 2020, **11**, 4722

All publication charges for this article have been paid for by the Royal Society of Chemistry

Transmembrane anion transport mediated by halogen bonding and hydrogen bonding triazole anionophores†

Laura E. Bickerton,  Alistair J. Sterling,  Paul D. Beer,  Fernanda Duarte * and Matthew J. Langton *

Transmembrane ion transport by synthetic anionophores is typically achieved using polar hydrogen bonding anion receptors. Here we show that readily accessible halogen and hydrogen bonding 1,2,3-triazole derivatives can efficiently mediate anion transport across lipid bilayer membranes with unusual anti-Hofmeister selectivity. Importantly, the results demonstrate that the iodo-triazole systems exhibit the highest reported activity to date for halogen bonding anionophores, and enhanced transport efficiency relative to the hydrogen bonding analogues. In contrast, the analogous fluoro-triazole systems, which are unable to form intermolecular interactions with anions, are inactive. The halogen bonding anionophores also exhibit a remarkable intrinsic chloride over hydroxide selectivity, which is usually observed only in more complex anionophore designs, in contrast to the readily accessible acyclic systems reported here. This highlights the potential of iodo-triazoles as synthetically accessible and versatile motifs for developing more efficient anion transport systems. Computational studies provide further insight into the nature of the anion-triazole intermolecular interactions, examining the origins of the observed transport activity and selectivity of the systems, and revealing the role of enhanced charge delocalisation in the halogen bonding anion complexes.

Received 11th March 2020

Accepted 14th April 2020

DOI: 10.1039/d0sc01467b

rsc.li/chemical-science

Introduction

The development of supramolecular anionophores for transmembrane ion transport is driven by their potential utility as tools for studying ion transport processes and as therapeutics for diseases arising from mis-regulation of protein ion channels.^{1–4} Significant effort has been devoted to designing mobile carrier systems with high anion transport activity in vesicles (particularly for chloride), and more recently, in cells.^{5–10} As with naturally occurring ion transporters, anion selectivity is crucial, and depends on the delicate balance between transporter anion binding selectivity and anion desolvation. Selectivity for chloride over proton transport (or the functionally equivalent hydroxide) is particularly necessary for applications in which dissipation of transmembrane pH gradients must be avoided. The naturally occurring anionophore, prodigiosin,¹¹ and its synthetic analogues,¹² are known to uncouple H⁺-ATPases or neutralise organelles by facilitated H⁺/Cl[−] symport, and for this reason are promising candidates for anti-cancer agents. Conversely, anionophores designed for treating diseases arising

from misregulated chloride channels, including cystic fibrosis and Bartter syndrome, must have high Cl[−] > H⁺/OH[−] selectivity to avoid toxicity arising from disrupting transmembrane pH gradients. However, designing transporters with such selectivity remains a significant challenge. Polar NH hydrogen bond (HB) donors (such as ureas or squaramides) which are typically used in supramolecular anionophores exhibit no intrinsic Cl[−] > H⁺/OH[−] selectivity.¹⁰ Improved chloride selectivity has been achieved by designing anionophores which encapsulate the anion, such as tripodal or cholapod-based receptors, but in general, more acidic NH HB-donors that are required for anion binding and efficient transport lead to decreased Cl[−] > H⁺/OH[−] selectivity.¹⁰

C–H hydrogen bonding or C–I halogen bonding (XB)^{13–15} interactions have recently emerged as potential alternatives to the classical N–H or O–H HB donors for anion transport. Compared to classical HB, these interactions are less hydrophilic, encounter diminished dehydration penalties, and are less inclined to promote detrimental transporter aggregation.¹⁶ XB in particular can exhibit superior anion binding affinity in competitive polar organic¹⁷ or aqueous media^{18–23} to hydrogen bonding,^{18–23} pointing to its potential utility in transmembrane anion transport systems. However, to date only a handful of XB-mediated anion transport systems have been reported, exploiting iodo-perfluoro alkane and arene derivatives for anion recognition and transport,^{24–28} and examples of transporters

Chemistry Research Laboratory, University of Oxford, Mansfield Road, Oxford, OX1 3TA, UK. E-mail: matthew.langton@chem.ox.ac.uk; fernanda.duartegonzalez@chem.ox.ac.uk

† Electronic supplementary information (ESI) available. See DOI: 10.1039/d0sc01467b



mediating anion transport solely through C–H HB interactions are also rare.^{16,29–31} The potential power of XB for anion transport was exemplified by Matile and co-workers who reported that gaseous iodotrifluoromethane facilitates anion transport when bubbled through the vesicle solution.²⁵

Herein we show that simple acyclic XB or HB triazoles (Fig. 1) can efficiently mediate anion transport across lipid bilayer membranes with an unusual anti-Hofmeister selectivity. Importantly, we demonstrate unprecedented activity for XB anionophores with up to two orders of magnitude improvement over the previously reported iodo-perfluorobenzene systems, and reveal their remarkable intrinsic $\text{Cl}^- > \text{OH}^-$ selectivity. Iodo- and proto-triazoles are versatile motifs readily accessible *via* Cu-catalysed azide–alkyne click chemistry,³² and these results demonstrate their potential for applications in synthetic anion transport systems.

Results and discussion

Synthesis and anion recognition properties

Acyclic 5-iodo/proto/fluoro-1,4-disubstituted-1,2,3-triazoles, of the general form shown in Fig. 1, were prepared as minimalistic scaffolds with which to explore the intrinsic activity and selectivity of the hydrophobic C–I XB- and C–H HB-mediated anion transport processes. The family of compounds spans a range of iodo-triazole derivatives, and their proto-triazole analogues, with varied electron-withdrawing/donating substituents on the aryl group and varying alkyl chain lengths. The library of 5-iodo-1,4-disubstituted-1,2,3-triazoles (compounds **1b–9b**) were prepared by Cu-catalysed azide–alkyne cycloaddition of the respective alkyl azide and iodo-aryl-alkyne, in the presence of tris[(1-benzyl-1*H*-1,2,3-triazol-4-yl)methyl]amine (TBTA) (Scheme 1). The analogous proto-triazoles (compounds **1a–9a**) were prepared from the corresponding alkyne. As control compounds, the fluoro-triazole analogues of **1** and **9**, namely **1c** and **9c**, which are unable to form HB or XB interactions, were also prepared from the corresponding iodo-triazole by heating with potassium fluoride. Full synthetic procedures and characterisation are available in the ESI†

The anion recognition capability of representative proto-triazole **1a** and iodo-triazole **1b** were first investigated by ^1H NMR binding titrations with $\text{Bu}_4\text{N}^+\text{X}^-$ in d_6 -acetone, monitoring the binding induced chemical shift perturbations of the proto-triazole *H* and adjacent aryl protons. For each anion, the data could be fitted to a 1 : 1 binding isotherm (see ESI†) and

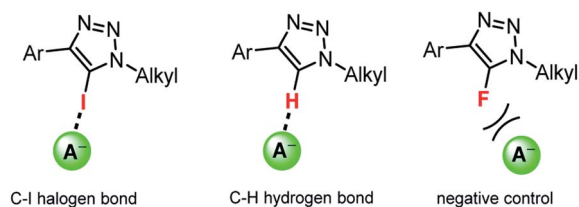
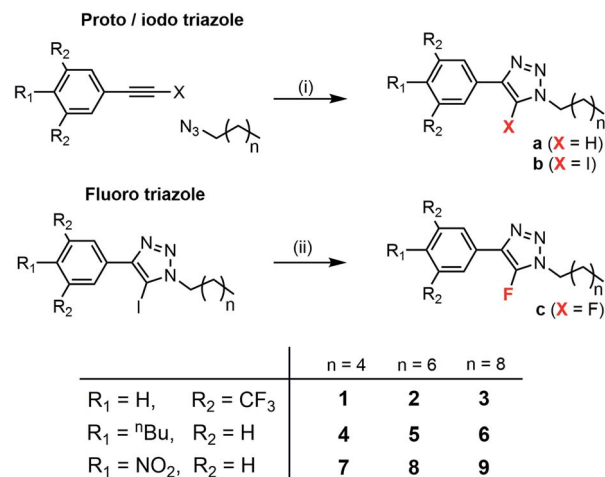


Fig. 1 Representative acyclic halogen bonding (XB) and hydrogen bonding (HB) triazole anion transporters, and the analogous fluoro-triazole negative controls.



Scheme 1 Synthesis of triazole derivatives and compound numbering scheme. Conditions (i) $\text{Cu}(\text{CH}_3\text{CN})_4\text{PF}_6$, TBTA, THF, N_2 , rt (ii) Kf, CH_3CN , μ -wave 180 °C.

the 1 : 1 stoichiometric association constants determined using the Bindfit program (Table 1).^{33,34} The data revealed an overall selectivity trend of $\text{Cl}^- > \text{Br}^- > \text{I}^-$ for both **1a** and **1b**, and approximately one order of magnitude enhancement of halide binding affinity for the XB iodo-triazole receptor **1b** compared to HB proto-triazole **1a**. For both compounds, no measurable binding of nitrate was observed under these conditions.

Transmembrane anion transport activity

The ability of anionophores **1–9a/b** to mediate OH^-/Cl^- transmembrane anion transport was first determined in 1-palmitoyl-2-oleoyl-*sn*-glycero-3-phosphocholine large unilamellar vesicles (POPC LUVs), loaded with 8-hydroxypyrene-1,3,6-trisulfonate (HPTS) and buffered to pH 7.0 in NaCl solution. HPTS is a pH-sensitive fluorophore, which allows for ratiometric determination of the internal pH of the LUVs. A pH gradient was applied across the membrane by addition of a base pulse, followed by addition of the carrier as a DMSO solution (<0.5% v/v). The ability of the anionophore to dissipate the pH gradient by transmembrane OH^-/Cl^- exchange was determined by recording the change in the HPTS emission, I_{rel} ($\lambda_{\text{em}} = 510 \text{ nm}$), with time following excitation at $\lambda_{\text{ex}} = 405/465 \text{ nm}$ (Fig. 2a). At the end of each experiment, excess detergent (Triton X-100) was

Table 1 Binding affinities for triazole derivatives **1a** and **1b**

	K_a/M^{-1}	
	1a	1b
Cl^-^a	17 ± 1	197 ± 14
Br^-^a	9 ± 7	110 ± 35
I^-^a	<3	38 ± 9
$\text{NO}_3^-^a$	— ^b	— ^b

^a Anions added as the TBA salt in d_6 -acetone, data fitted to a 1 : 1 binding model using Bindfit. ^b Perturbations too small to obtain binding constant. Errors at the 95% confident limit.



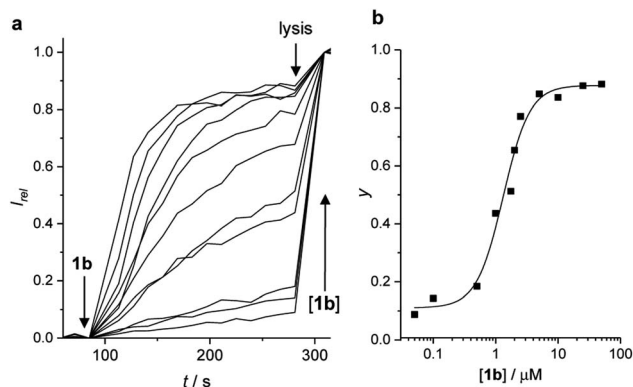


Fig. 2 Anion transport by XB transporter **1b** in the HPTS assay. (a) Change in ratiometric emission ($\lambda_{\text{em}} = 510$ nm; $\lambda_{\text{ex1}} = 405$ nm, $\lambda_{\text{ex2}} = 460$ nm) upon addition of **1b** in DMSO (0.05–50 μM) to POPC vesicles containing 1 mM HPTS, 100 mM internal and external NaCl, buffered with 10 mM HEPES at pH 7.0. A pH gradient is generated by addition of a NaOH base pulse (0.5 M), followed by **1b** at $t = 0$. Vesicle lysis by Triton X-100 calibrates the assay. (b) Dependence on fractional activities (y , the relative intensity at $t = 288$ s just prior to lysis) on concentration of **1b** (black squares), and fit to the Hill equation (black line).

added to lyse the vesicles for calibration of the emission intensity. The HPTS assay was used to determine the concentration dependence of the activity of each anion carrier. Fig. 2a shows representative data for the activity of compound **1b** at a range of concentrations. The fractional activities (y , the relative intensity at 288 s, immediately prior to lysis) were plotted as a function of concentration (Fig. 2b) and fitted to the Hill equation (eqn (1)). Original data for all other compounds is available in the ESI.†

The Hill equation here is used to describe the dependence of the fractional activities y on the n^{th} power of the anionophore

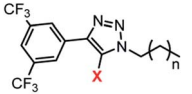
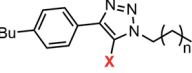
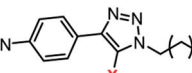
concentration x , and facilitates comparison of the relative activities of transporters through an effective concentration value (EC_{50}) required to reach 50% activity in the given assay (eqn (1)). Compatibility with the Hill equation reveals endergonic self-assembly of the active supramolecule, and Hill coefficients $n > 1$ are indicative of the stoichiometry of the unstable supramolecular assembly that exists in the presence of an excess of uncomplexed anionophores.³⁵

$$y = y_0 + (y_{\text{max}} - y_0) \frac{x^n}{\text{EC}_{50}^n + x^n} \quad (1)$$

EC_{50} values, hill coefficients and calculated partition coefficients ($\log P$) values for the proto- and iodo-triazoles are shown in Table 2. $\log P$ values were calculated using the VCCLab software.³⁶

In general, the electron withdrawing 3,5-bis(trifluoromethyl)benzene and 4-nitrobenzene substituents led to excellent activity despite the simplicity of the anionophores (compounds **1–3**, and **7–9**, respectively). The electron deficient halogen bonding transporters **1b** and **9b** are approximately $3\times$ more active than the most active XB anionophore reported to date, iodoperfluorohexane ($\text{EC}_{50} = 3.1$ μM);²⁵ and notably over two orders of magnitude more active than the archetypal XB donor iodoperfluorobenzene under comparable assay conditions ($\text{EC}_{50} = 260$ μM).^{25,28} Electron donating 4-*n*-butylbenzene substituents (compounds **4–6**) conversely decreased activity, consistent with the expected decreased XB and HB donor strength. The correlation between activity and $\log P$ is complex, because transport efficiency is also strongly dependent on other factors including anion binding affinity and molecular size, which are not easily decoupled.³⁷ Nevertheless, the observed trend of maximum activity of compounds with $\log P$ of 4–6, and reduced activity observed for compounds with higher and lower lipophilicities, is broadly consistent with previous reports on

Table 2 Characteristics of the HB and XB anion transporters

		$n = 4$		$n = 6$		$n = 8$	
		X = H	X = I	X = H	X = I	X = H	X = I
	$\text{EC}_{50}^a/\mu\text{M}$	1a	1b	2a	2b	3a	3b
	n^b	2.0 (0.1)	1.3 (0.1)	0.9 (0.1)	1.1 (0.1)	>100	>100
	$\text{clog } P^c$	2.4 (0.3)	2.1 (0.4)	3.7 (0.8)	2.6 (0.4)	— ^d	— ^d
	$\text{EC}_{50}^a/\mu\text{M}$	4a	4b	5a	5b	6a	6b
	n^b	6.2 (0.2)	3.3 (0.2)	>200	>200	>200	>200
	$\text{clog } P^c$	5.6 (0.5)	2.0 (0.2)	— ^d	— ^d	— ^d	— ^d
	$\text{EC}_{50}^a/\mu\text{M}$	7a	7b	8a	8b	9a	9b
	n^b	14.8 (0.4)	1.8 (0.2)	2.9 (0.2)	3.6 (0.3)	2.7 (0.05)	1.2 (0.1)
	$\text{clog } P^c$	5.7 (0.8)	3.1 (0.7)	3.6 (0.7)	2.7 (0.6)	7.7 (1.2)	2.0 (0.2)
		3.9	4.4	4.8	5.2	5.6	6.0

^a Effective concentration to reach 50% of maximal activity in the HPTS assay, determined from Hill analysis of the relative fluorescence intensity at $t = 288$ s, immediately prior to vesicle lysis. Experiments conducted in LUVs of POPC (mean diameter 200 nm) loaded with 1 mM HPTS, NaCl (100 mM) and buffered at pH 7.0 with 10 mM HEPES. For compounds of low activity, estimated lower bounds for the EC_{50} value are given. ^b Hill coefficient. ^c Calculated $\log P$. ^d Insufficient activity for Hill analysis.

the role of lipophilicity on HB-mediated anion carriers.³⁸ For compounds in which both XB and HB derivatives fall within these optimum parameters (compounds **1**, **4**, **7** and **8**), a general enhancement of activity of around 2×, and up to 8×, is observed for XB systems over their HB analogues. The most lipophilic transporters (**3**, **5**, **6**) are inactive, likely arising from reduced mobility and reorganization of longer chain derivatives within the lipid bilayer.³⁹

Calculation of the electrostatic potential (ESP) surface for methyl-truncated analogues† of **1a/b**, **4a/b** and **7a/b** (denoted **1a'/b'**, **4a'/b'** and **7a'/b'** respectively) reveals the characteristic iodine-centred sigma-hole^{40,41} associated with halogen bonding donors, and the accumulation of δ+ surrounding the triazole protons active in hydrogen bonding (Fig. 3). Comparison of the Hammett σ values for each substituent demonstrate that the more electron-withdrawing substituents result in a more positive value for the ESP maximum, leading to a stronger XB/HB-anion intermolecular interaction. This correlates with the observed greater activity of **1a/b** and **7a/b** over **4a/b** (Table 2).

Evidence for XB/HB-anion interactions and mobile carrier mechanism

To confirm the role of the C–I XB and C–H HB interactions in the anion transport process, we investigated the anion transport capability of fluoro-triazole derivative **1c**, which is unable to form XB or HB interactions through the triazole motif. Inactivity of **1c** in the HPTS assay confirmed the role of the XB and HB intermolecular interactions in the transport processes (Fig. 4a). Similar behaviour was observed for nitro-phenyl fluoro-triazole derivative **9c**.

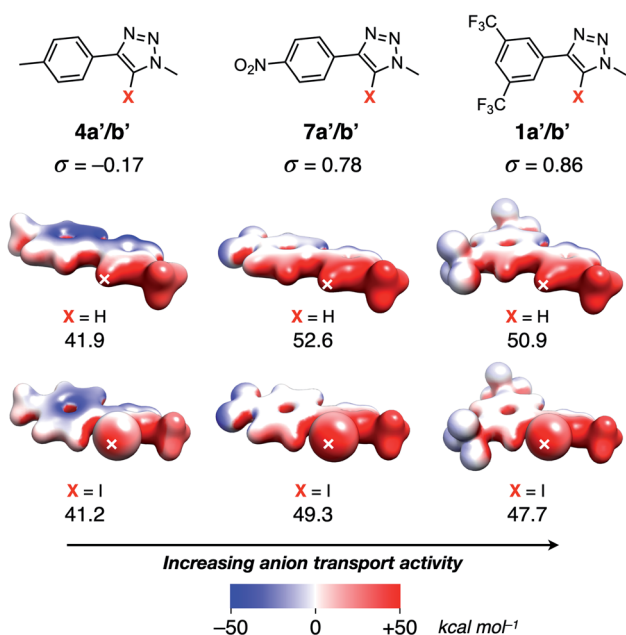


Fig. 3 Calculated electrostatic potential surfaces (isovalue = 0.04 a.u.) for truncated transporter ligands **4a'/b'**, **7a'/b'** and **1a'/b'** calculated at the SMD(CHCl₃)- ω B97X-D/def2-TZVP level of theory. Maximum ESP values are located at the position of each cross, and reported beneath each transporter in kcal mol⁻¹.

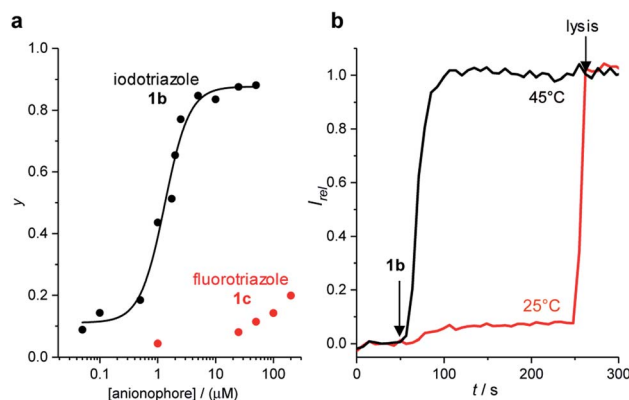


Fig. 4 (a) Activity of fluoro-triazole **1c** (red) in comparison with iodo-triazole **1b** (black) in the HPTS assay. Plot shows dependence on I_{rel} at $t = 288$ s immediately prior to lysis on anionophore concentration (points) and fit to the Hill equation (line). (b) Temperature dependence of anion transport by **1b** (2 μ M) in DPPC lipid vesicles in the HPTS assay at 25 °C (black line) and 45 °C (red line).

Inactivity of the transport systems **1–9** reported here in the carboxyfluorescein dye leakage assay rules out non-specific leakage by these systems (ESI†). Replacement of the zwitterionic POPC lipids in the HPTS assay with anionic egg yolk phosphatidylglycerol (EYPG) lipids led to a significant decrease in observed activity, consistent with the requirement for formation of an anionic complex in the rate limiting transport process. Transport activity at 25 °C with XB transporter **1b** and dipalmitoylphosphatidylcholine (DPPC) lipids, under otherwise identical conditions, was negligible (Fig. 4b). The lipid gel phase inhibits translation of mobile carriers through the membrane which are otherwise mobile in a fluid lipid phase. The gel to fluid phase transition for DPPC lipids is 41 °C, and repeating the assay above this temperature (45 °C) restored anion transport activity. The observed temperature dependence is indicative of a mobile carrier mechanism, and rules out formation of a membrane-spanning supramolecular channel structure whose activity would be independent of the lipid phase.

Anion selectivity

Dissipation of the transmembrane pH gradient measured in the HPTS assay by the carrier species can in principle occur through either cation (H^+/M^+) or anion (OH^-/A^-) antiport (exchange), or H^+/A^- symport (co-transport) mechanisms. The activities of HB transporter **1a** and XB transporter **1b** were not affected by iso-osmolar replacement of the external Na^+ cation with Li^+ , K^+ , Rb^+ or Cs^+ (see ESI†), indicative of selective anion transport (OH^-/A^- antiport or H^+/A^- symport) rather than H^+/M^+ cation antiport. Further evidence to support the cation-independent transport mechanism was provided by conducting analogous experiments in the presence of sodium gluconate, a large hydrophilic anion (ESI†).¹⁰ The absence of detectable transport indicates that, as expected, neither OH^- /gluconate antiport or H^+ /gluconate symport mechanisms are active because of the insurmountable dehydration penalty of gluconate, and also that the alternative H^+/Na^+ cation antiport process is negligible.

OH^-/A^- antiport and H^+/A^- symport mechanisms are functionally equivalent and cannot be distinguished through these transport assays. However, the low basicity of triazole derivatives ($\text{p}K_{\text{a}}\text{H} \sim 0\text{--}1$)⁴³ suggests that H^+/A^- symport (achieved *via* triazole protonation and XB/HB-mediated anion recognition) is unlikely to contribute to any significant extent to the ion transport process at neutral pH. This is consistent with the activity of previously reported XB iodoalkene/arene transporters in the same assay, which do not possess any basic atoms and are therefore most likely operate through an anion antiport mechanism.²⁵ For simplicity, we refer to the transport process from here on in as OH^-/A^- antiport.

To examine the relative rates of Cl^- vs. OH^- transport, we repeated the HPTS assay with the addition of cyanide-*p*-trifluoromethoxyphenylhydrazone (FCCP), a weak acid protonophore at a low concentration (0.25 μM) insufficient to cause activity alone. FCCP transports protons *via* transmembrane shuttling of both protonated and deprotonated forms of the molecule. Enhancement of activity by FCCP is indicative of a rate limiting electrogenic OH^- transport process, because FCCP decouples the anionophore-mediated OH^-/Cl^- antiport process (Fig. 5a) by facilitating rapid electrogenic H^+ transport in an overall coupled Cl^-/H^+ symport process (Fig. 5b). In this scenario, the observed rate of pH gradient dissipation reports on the rate-limiting electrogenic Cl^- transport process. As such, if the activity of a given carrier is invariant to FCCP addition, Cl^- transport must therefore be rate limiting in the antiport mechanism (*i.e.* slower than electrogenic OH^- transport). The EC_{50} values for compounds **1a** and **1b** with FCCP are shown in Table 3. The activity of HB anionophore is invariant to FCCP addition, demonstrating rapid OH^- transport and rate limiting Cl^- transport by **1a**. In contrast, a four-fold increase in activity for XB transporter **1b** is observed in the presence of FCCP, revealing rate limiting OH^- transport in its absence. The ratio of EC_{50} values in the absence and presence of FCCP (Table 3, column 4) therefore reports on the relative $\text{Cl}^- > \text{OH}^-$ selectivity of the system (for the given conditions and ion concentration gradient), and reveals the unusual $\text{Cl}^- > \text{OH}^-$ selectivity of the XB transporter **1b**. Notably, transporter **1b** in the presence of FCCP achieved nanomolar activity ($\text{EC}_{50} = 300 \text{ nM}$) in the HPTS assay, which to the best of our knowledge is the highest activity reported to date for an XB anion transporter under comparable experimental conditions. This highlights the potential of iodo-triazoles as synthetically accessible and versatile motifs for developing more efficient anion transport systems.

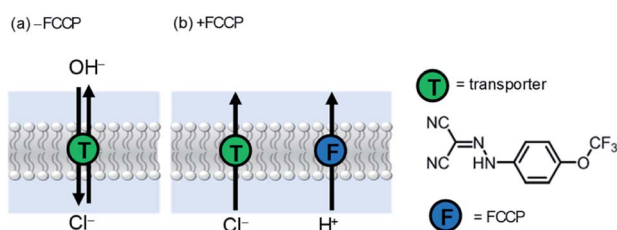


Fig. 5 Ion transport mechanisms for anionophore-mediated dissipation of a transmembrane pH gradient (a) in the absence and (b) presence of cyanide-*p*-trifluoromethoxyphenylhydrazone (FCCP).

Table 3 FCCP dependence of transporters **1a** and **1b**

	$\text{EC}_{50}^a/\mu\text{M}$	$\text{EC}_{50}^{\text{FCCP}b}/\mu\text{M}$	$\text{EC}_{50}/\text{EC}_{50}^{\text{FCCP}}$
1a	2.0 ± 0.1	2.2 ± 0.5	0.9
1b	1.3 ± 0.1	0.3 ± 0.05	4

^a EC_{50} in the absence of FCCP. ^b EC_{50} in the presence of 0.25 μM FCCP.

In the presence of FCCP, the observed transport kinetics report on the rate limiting A^- transport for a given anionophore. This allows the relative selectivity of both XB and HB transporters for each anion to be investigated, enabling direct comparison of the relative rates of electrogenic A^- transport (Fig. 6). HB transporter **1a** exhibits an overall selectivity profile of $\text{Cl}^- > \text{Br}^- > \text{I}^- > \text{NO}_3^-$ (Fig. 6, black data). This selectivity is remarkable because in general hydrogen bonding anion transporters exhibit Hofmeister selectivity, whereby more weakly hydrated anions are selectively transported across the membrane due to ease of desolvation.^{44–47} The analogous XB anionophore **1b** exhibits a selectivity profile of $\text{NO}_3^- > \text{Cl}^- > \text{Br}^- > \text{I}^-$. Comparison of the relative activities for both transporters in the absence of FCCP allows placement of OH^- into the overall selectivity trends, revealing $\text{OH}^- > \text{Cl}^- > \text{Br}^- > \text{I}^- > \text{NO}_3^-$ behaviour for **1a** and $\text{NO}_3^- > \text{Cl}^- > \text{Br}^- > \text{OH}^- > \text{I}^-$ behaviour for **1b**. Similar selectivity trends for analogous compounds **9a** and **9b** were also observed in these assays (see ESI†).

Overall these transport experiments reveal (i) enhanced activity of halogen bonding anionophores vs. hydrogen bonding analogues across all anions, (ii) unusual $\text{Cl}^- > \text{OH}^-$ selectivity for the halogen bonding anionophores and (iii) anti-Hofmeister bias for halide transport, demonstrating the dominant role of ion binding to the anionophore and correlating with NMR determined anion binding affinities (see Table 1).§

Computational studies into anionophore–anion interactions

Computational studies were used to probe the binding energies and structures of the anionophore–anion complexes.

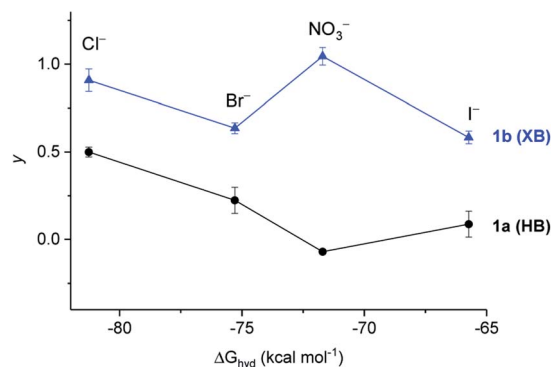


Fig. 6 Dependence of the activity of **1a** (black circles) and **1b** (blue triangle) on the hydration energy ΔG_{hyd} of extravesicular anions (100 mM NaX, inside 100 mM NaCl) in the presence of 0.25 μM protonophore FCCP, reporting on relative rate of electrogenic X^- transport. Error bars represent standard deviations.



Calculation^{48–53} of the relative binding enthalpies for both 1 : 1 and 2 : 1 model anionophore–anion complexes in CHCl_3 implicit solvent as a membrane-mimetic environment reveals that $\Delta H_{\text{bind}}(2 : 1) > 2 \times \Delta H_{\text{bind}}(1 : 1)$ (Fig. 7), and that 2 : 1 binding is enhanced by π -stacking between the arenes (see ESI†).[†] Bidentate binding was found to be preferred in the model 1 : 1 HB system **1a'** involving hydrogen bonds from both the alkyl $\text{C}(\text{sp}^3)\text{--H1}$ and triazole $\text{C}(\text{sp}^2)\text{--H2}$ (Fig. 7a). This finding is in line with the result of the ESP calculations in Fig. 3. Monodentate XB interactions are observed with **1b'** (Fig. 7b). Interestingly, our results indicate that in the 2 : 1 complex, four HB $\text{C--H}\cdots\text{anion}$ interactions per anion exists for **1a'** (Fig. 7a), while only one XB $\text{C--I}\cdots\text{anion}$ interaction is present for **1b'** (Fig. 7b).

Additionally, bond order and second-order perturbation theory analysis, which allows the quantification of bond energies ($E^{(2)}$)⁵⁴ indicates that addition of the second transporter ligand weakens the total XB interactions compared with the 1 : 1 complex ($E_{\text{XB}}^{(2)} = 40.6$ vs. $30.7 \text{ kcal mol}^{-1}$). However, this is partially compensated by dispersion interactions between the two transporter ligands ($E_{\text{T1--T2}} = 16.0 \text{ kcal mol}^{-1}$) and a C–H interaction ($10.1 \text{ kcal mol}^{-1}$), which leads to an overall larger stabilisation energy ($E_{\text{total}}^{(2)} = 56.8 \text{ kcal mol}^{-1}$).

Analysis of the partial charges on each anion in the 1 : 1 and 2 : 1 binding modes suggest a correlation between the rate of transport and the ability of the transporter to stabilise the anion

charge (Fig. 8). For example, for Cl^- , Br^- and I^- , the negative charge is more effectively delocalised over the XB anionophore than the HB analogue. This is consistent with previous results from Donor K-edge X-ray Absorption Spectroscopy experiments which revealed significant covalency in the XB interaction between related iodo-triazole XB donors and chloride anions (comparable to that in transition metal chloride complexes), in contrast to proto-triazole analogues with negligible charge transfer contribution to the HB interaction.⁵⁵ Improved charge

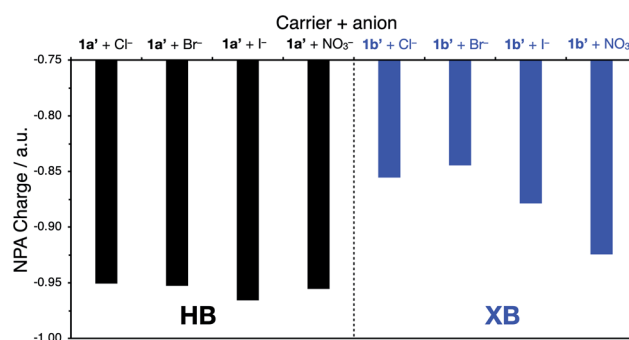


Fig. 8 Partial charges on each anion for 1 : 1 anionophore–anion complexes of **1a'** and **1b'**, calculated using natural population analysis (NPA) at the [NBO/SMD(CHCl_3)- ω B97X-D3/def2-SVP (ma-def2-SVP on anion)] level of theory.

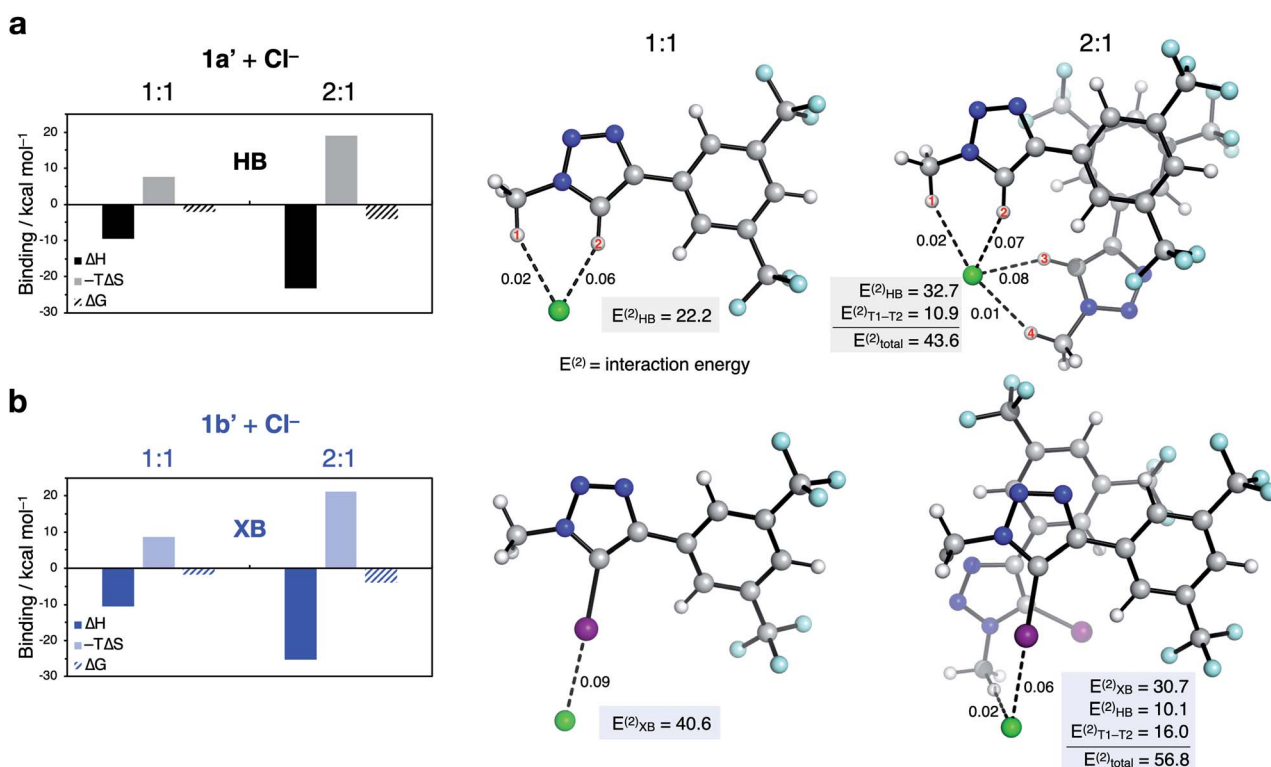


Fig. 7 Characterisation of 1 : 1 and 2 : 1 binding of (a) **1a'** and (b) **1b'** to chloride. Enthalpies, entropies and free energies of binding (kcal mol^{-1}) were calculated at the [SMD(CHCl_3)-DLPNO-CCSD(T)/def2-TZVP (ma-def2-TZVP on Cl, I)/ ω B97X-D3/def2-SVP (ma-def2-SVP on Cl, I)] level of theory. Mayer bond orders (dashed lines), their associated HB/XB bond energies ($E_{\text{HB/XB}}^{(2)}$), and interaction energy between ligands ($E_{\text{T1--T2}}^{(2)}$) in kcal mol^{-1} were calculated at the [NBO/SMD(CHCl_3)- ω B97X-D3/def2-SVP (ma-def2-TZVP on Cl, I)/ ω B97X-D3/def2-SVP (ma-def2-SVP on Cl, I)] level of theory. Free energies were calculated using a quasi-RRHO approximation⁵³ and corrected for a 1 M standard state at 298.15 K.

delocalisation over the anion-triazole complex is expected to decrease the barrier to transport across the hydrophobic membrane (Fig. 8), and this is consistent with the experimentally observed selectivity trend of the XB anionophores enhancing rates of anion transport over the analogous HB system. A different behaviour is observed for nitrate, where the observed efficient nitrate transport does not correlate with the increased calculated partial charge. We suggest that this behaviour is due to the greater number of thermally-accessible conformations for the binding of the trigonal nitrate anion, each of them having a different charge distribution. In this case, the most stable conformer in solution is likely not the most active for membrane transport (see ESI†).

Conclusions

We have shown that acyclic halogen bonding iodo-triazoles can efficiently transport anions across lipid bilayer membranes, with enhanced activity in comparison to hydrogen bonding proto-triazole analogues. Despite the relative simplicity of the design, the iodo-triazole systems are the most active halogen bonding anionophores reported to date. Anion transport experiments reveal unusual anti-Hofmeister selectivities, and a remarkable intrinsic $\text{Cl}^- > \text{OH}^-$ selectivity for the halogen bonding systems. Experimental and computational studies provide further insight into the binding modes of the anion-anionophore complexes. Calculations demonstrate that the strength of the non-covalent interactions are sufficient to overcome the entropic cost of 2 : 1 complex formation, and reveal the remarkable ability of the halogen bonding anionophores to delocalise the anion charge over the complex, which correlates with the enhanced anion transport capability observed by experiment. This work demonstrates the utility of the synthetically accessible and highly versatile XB and HB triazole motif for anionophore design. The observed $\text{Cl}^- > \text{OH}^-$ selectivity of the iodotriazole derivatives also suggest that such motifs may provide the starting point for designing novel ionophores with enhanced selectivity for potential future application in channelopathy therapeutics.

Conflicts of interest

There are no conflicts to declare.

Acknowledgements

A. J. S. thanks the EPSRC Centre for Doctoral Training in Synthesis for Biology and Medicine for a studentship (EP/L015838/1), generously supported by AstraZeneca, Diamond Light Source, Defence Science and Technology Laboratory, Evotec, GlaxoSmithKline, Janssen, Novartis, Pfizer, Syngenta, Takeda, UCB and Vertex. A. J. S. also thanks the Oxford-Radcliffe Scholarship for a studentship. A. J. S. and F. D. thank the EPSRC Centre for Doctoral Training for Theory and Modelling in Chemical Sciences (EP/L015722/1) for providing access to the Dirac cluster at Oxford. This work used the Cirrus UK National Tier-2 HPC Service at EPCC (<http://www.cirrus.ac.uk>) funded by

the University of Edinburgh and EPSRC (EP/P020267/1). M. J. L. acknowledges funding from the Royal Society. F. D. and M. J. L. thank the John Fell Oxford University Press Research Fund for financial support. M. J. L. is a Royal Society University Research Fellow.

Notes and references

‡ Truncated alkyl chains to methyl were used for computational studies. This does not affect the calculated ESP (see ESI† for details).

§ Detailed comparison between the measured association constants in solution and transport kinetics in membranes should be avoided, given that the observed rate of transport is also dependent on many other factors including desolvation, anionophore-ion complex mobility in the membrane, and competing binding interactions of the transporter with the phosphate head groups.³⁷

¶ Discussed here are the lowest energy conformers obtained from the sampling procedure described in the ESI.†

- 1 A. P. Davis, D. N. Sheppard and B. D. Smith, *Chem. Soc. Rev.*, 2007, **36**, 348–357.
- 2 J. T. Davis, O. Okunola and R. Quesada, *Chem. Soc. Rev.*, 2010, **39**, 3843–3862.
- 3 S. Matile, A. V. Jentzsch, J. Montenegro and A. Fin, *Chem. Soc. Rev.*, 2011, **40**, 2453–2474.
- 4 P. A. Gale, J. T. Davis and R. Quesada, *Chem. Soc. Rev.*, 2017, **46**, 2497–2519.
- 5 B. Díaz de Greñu, P. I. Hernández, M. Espona, D. Quiñonero, M. E. Light, T. Torroba, R. Pérez-Tomás and R. Quesada, *Chem.–Eur. J.*, 2011, **17**, 14074–14083.
- 6 B. Shen, X. Li, F. Wang, X. Yao and D. Yang, *PLoS One*, 2012, **7**, e34694.
- 7 S.-K. Ko, S. K. Kim, A. Share, V. M. Lynch, J. Park, W. Namkung, W. Van Rossom, N. Busschaert, P. A. Gale, J. L. Sessler and I. Shin, *Nat. Chem.*, 2014, **6**, 885–892.
- 8 V. Soto-Cerrato, P. Manuel-Manresa, E. Hernando, S. Calabuig-Fariñas, A. Martínez-Romero, V. Fernández-Dueñas, K. Sahlholm, T. Knöpfel, M. García-Valverde, A. M. Rodilla, E. Jantus-Lewintre, R. Farràs, F. Ciruela, R. Pérez-Tomás and R. Quesada, *J. Am. Chem. Soc.*, 2015, **137**, 15892–15898.
- 9 H. Li, H. Valkenier, L. W. Judd, P. R. Brotherhood, S. Hussain, J. A. Cooper, O. Jurček, H. A. Sparkes, D. N. Sheppard and A. P. Davis, *Nat. Chem.*, 2016, **8**, 24–32.
- 10 X. Wu, L. W. Judd, E. N. W. Howe, A. M. Withecombe, V. Soto-Cerrato, H. Li, N. Busschaert, H. Valkenier, R. Pérez-Tomás, D. N. Sheppard, Y.-B. Jiang, A. P. Davis and P. A. Gale, *Chem*, 2016, **1**, 127–146.
- 11 S. Ohkuma, T. Sato, M. Okamoto, H. Matsuya, K. Arai, T. Kataoka, K. Nagai and H. H. Wasserman, *Biochem. J.*, 1998, **334**, 731–741.
- 12 P. I. Hernández, D. Moreno, A. A. Javier, T. Torroba, R. Pérez-Tomás and R. Quesada, *Chem. Commun.*, 2012, **48**, 1556–1558.
- 13 P. Metrangolo, F. Meyer, T. Pilati, G. Resnati and G. Terraneo, *Angew. Chem., Int. Ed.*, 2008, **47**, 6114–6127.
- 14 T. M. Beale, M. G. Chudzinski, M. G. Sarwar and M. S. Taylor, *Chem. Soc. Rev.*, 2013, **42**, 1667–1680.



- 15 L. C. Gilday, S. W. Robinson, T. A. Barendt, M. J. Langton, B. R. Mullaney and P. D. Beer, *Chem. Rev.*, 2015, **115**, 7118–7195.
- 16 M. Lisbjerg, H. Valkenier, B. M. Jessen, H. Al-Kerdi, A. P. Davis and M. Pittelkow, *J. Am. Chem. Soc.*, 2015, **137**, 4948–4951.
- 17 C. C. Robertson, R. N. Perutz, L. Brammer and C. A. Hunter, *Chem. Sci.*, 2014, **5**, 4179–4183.
- 18 M. J. Langton, S. W. Robinson, I. Marques, V. Félix and P. D. Beer, *Nat. Chem.*, 2014, **6**, 1039–1043.
- 19 M. J. Langton, I. Marques, S. W. Robinson, V. Félix and P. D. Beer, *Chem.–Eur. J.*, 2016, **22**, 185–192.
- 20 C. J. Massena, N. B. Wageling, D. A. Decato, E. Martin Rodriguez, A. M. Rose and O. B. Berryman, *Angew. Chem., Int. Ed.*, 2016, **55**, 12398–12402.
- 21 C. J. Massena, D. A. Decato and O. B. Berryman, *Angew. Chem., Int. Ed.*, 2018, **57**, 16109–16113.
- 22 T. Bunchuay, A. Docker, A. J. Martinez-Martinez and P. D. Beer, *Angew. Chem., Int. Ed.*, 2019, **58**, 13823–13827.
- 23 A. Borissov, I. Marques, J. Y. C. Lim, V. Félix, M. D. Smith and P. D. Beer, *J. Am. Chem. Soc.*, 2019, **141**, 4119–4129.
- 24 A. Vargas Jentzsch, D. Emery, J. Mareda, P. Metrangolo, G. Resnati and S. Matile, *Angew. Chem., Int. Ed.*, 2011, **50**, 11675–11678.
- 25 A. V. Jentzsch, D. Emery, J. Mareda, S. K. Nayak, P. Metrangolo, G. Resnati, N. Sakai and S. Matile, *Nat. Commun.*, 2012, **3**, 905.
- 26 A. Vargas Jentzsch and S. Matile, *J. Am. Chem. Soc.*, 2013, **135**, 5302–5303.
- 27 C. Ren, X. Ding, A. Roy, J. Shen, S. Zhou, F. Chen, S. F. Y. Li, H. Ren, Y. Yan Yang and H. Zeng, *Chem. Sci.*, 2018, **9**, 4044–4051.
- 28 L. M. Lee, M. Tsemperouli, A. I. Poblador-Bahamonde, S. Benz, N. Sakai, K. Sugihara and S. Matile, *J. Am. Chem. Soc.*, 2019, **141**, 810–814.
- 29 J. Shang, W. Si, W. Zhao, Y. Che, J.-L. Hou and H. Jiang, *Org. Lett.*, 2014, **16**, 4008–4011.
- 30 S. Chen, S. Zhang, C. Bao, C. Wang, Q. Lin and L. Zhu, *Chem. Commun.*, 2016, **52**, 13132–13135.
- 31 H. Valkenier, O. Akrawi, P. Jurček, K. Sleziaková, T. Lízal, K. Bartik and V. Šindelář, *Chem*, 2019, **5**, 429–444.
- 32 B. Schulze and U. S. Schubert, *Chem. Soc. Rev.*, 2014, **43**, 2522–2571.
- 33 BindFit v0.5 | Supramolecular, <http://app.supramolecular.org/bindfit/>.
- 34 D. B. Hibbert and P. Thordarson, *Chem. Commun.*, 2016, **52**, 12792–12805.
- 35 S. Bhosale and S. Matile, *Chirality*, 2006, **18**, 849–856.
- 36 I. V. Tetko, J. Gasteiger, R. Todeschini, A. Mauri, D. Livingstone, P. Ertl, V. A. Palyulin, E. V. Radchenko, N. S. Zefirov, A. S. Makarenko, V. Y. Tanchuk and V. V. Prokopenko, *J. Comput.-Aided Mol. Des.*, 2005, **19**, 453–463.
- 37 N. Busschaert, S. J. Bradberry, M. Wenzel, C. J. E. Haynes, J. R. Hiscock, I. L. Kirby, L. E. Karagiannidis, S. J. Moore, N. J. Wells, J. Herniman, G. J. Langley, P. N. Horton, M. E. Light, I. Marques, P. J. Costa, V. Félix, J. G. Frey and P. A. Gale, *Chem. Sci.*, 2013, **4**, 3036–3045.
- 38 V. Saggiomo, S. Otto, I. Marques, V. Félix, T. Torroba and R. Quesada, *Chem. Commun.*, 2012, **48**, 5274–5276.
- 39 S. J. Edwards, I. Marques, C. M. Dias, R. A. Tromans, N. R. Lees, V. Félix, H. Valkenier and A. P. Davis, *Chem.–Eur. J.*, 2016, **22**, 2004–2011.
- 40 P. Politzer, J. S. Murray and T. Clark, *Phys. Chem. Chem. Phys.*, 2013, **15**, 11178–11189.
- 41 J. Y. C. Lim and P. D. Beer, *Chem*, 2018, **4**, 731–783.
- 42 C. Hansch, A. Leo and R. W. Taft, *Chem. Rev.*, 1991, **91**, 165–195.
- 43 J.-L. M. Abboud, C. Foces-Foces, R. Notario, R. E. Trifonov, A. P. Volovodenco, V. A. Ostrovskii, I. Alkorta and J. Elguero, *Eur. J. Inorg. Chem.*, 2001, **2001**, 3013–3024.
- 44 S. K. Berezin and J. T. Davis, *J. Am. Chem. Soc.*, 2009, **131**, 2458–2459.
- 45 S. K. Berezin, *Supramol. Chem.*, 2013, **25**, 323–334.
- 46 Y. Yang, X. Wu, N. Busschaert, H. Furuta and P. A. Gale, *Chem. Commun.*, 2017, **53**, 9230–9233.
- 47 X. Wu, J. R. Small, A. Cataldo, A. M. Withecombe, P. Turner and P. A. Gale, *Angew. Chem., Int. Ed.*, 2019, **58**, 15142–15147.
- 48 F. Neese, *Wiley Interdiscip. Rev.: Comput. Mol. Sci.*, 2012, **2**, 73–78.
- 49 C. Riplinger and F. Neese, *J. Chem. Phys.*, 2013, **138**, 034106.
- 50 J.-D. Chai and M. Head-Gordon, *Phys. Chem. Chem. Phys.*, 2008, **10**, 6615–6620.
- 51 F. Weigend and R. Ahlrichs, *Phys. Chem. Chem. Phys.*, 2005, **7**, 3297–3305.
- 52 A. V. Marenich, C. J. Cramer and D. G. Truhlar, *J. Phys. Chem. B*, 2009, **113**, 6378–6396.
- 53 S. Grimme, *Chem.–Eur. J.*, 2012, **18**, 9955–9964.
- 54 E. D. Glendening, J. K. Badenhoop, A. E. Reed, J. E. Carpenter, J. A. Bohmann, C. M. Morales, P. Karafiloglou, C. R. Landis, and F. Weinhold, *NBO 7.0*, Theoretical Chemistry Institute, University of Wisconsin, Madison, WI, 2018.
- 55 S. W. Robinson, C. L. Mustoe, N. G. White, A. Brown, A. L. Thompson, P. Kennepohl and P. D. Beer, *J. Am. Chem. Soc.*, 2015, **137**, 499–507.

